Angular-resolved uv photoemission and the band structure of GeS

T. Grandke and L. Ley
Max-Planck-Institut für Festkörperforschung, 7000 Stuttgart, Federal Republic of Germany
(Received 7 January 1977)

Angular-resolved photoelectron spectra (ARPES) are presented for GeS using 21-eV excitation energy. From the measurements that cover a wide range of angles along the two principal directions in the basal plane of the orthorhombic layered compound GeS E vs $\vec{k}_{\parallel}$ curves were constructed. The band structure of GeS was calculated utilizing the empirical pseudopotential method. The E vs $\vec{k}_{\parallel}$ curves can almost completely be understood in terms of this band structure under the assumption that only *peaks* in the one-dimensional density of states along $k_{\perp}$ contribute significantly to the ARPES spectrum.

I. INTRODUCTION

The notion[1] that angular-resolved photoelectron spectra (ARPES) from single crystals would yield a more detailed picture of the electronic states than the conventional type of angle-integrated spectroscopy has led to a number of such measurements over recent years.[2] One of the basic concepts invoked to interpret these measurements is the conservation of electron momentum parallel to the surface during the escape of the hot electron from the crystal. The simultaneous determination of electron energy and escape direction defines this parallel momentum component $\vec{k}_{\parallel}$ and allows a localization of initial states of given energy E_i along a line defined by $\vec{k}_{\parallel}$ = const in the Brillouin zone (BZ). The lack of direct information on the momentum component $k_{\perp}$ perpendicular to the surface is least cumbersome for systems with negligible energy dispersion along $k_{\perp}$. It is therefore not surprising that with few exceptions[3] ARPES measurements have been made on layered compounds with $k_{\perp}$ kept perpendicular to the layers. The encouraging results of these measurements on systems with well-known band structure has led us to employ the method for the investigation of the band structure of GeS, a semiconducting IV-VI compound with layered structure.

The dielectric properties of GeS covering the range from infrared to the far uv have been determined from optical and electron energy-loss measurements.[4] Angle-integrated photoelectron spectra provide a reliable picture of the valence density of states[5] but no band structure is as yet available to interpret these data in detail.

In this paper we present the results of a band-structure calculation for GeS using the empirical pseudopotential method (EPM). The parameters of the calculation were adjusted to reproduce a band gap consistent with the optical measurements as well as the main features of the valence bands as determined by ARPES.

The details of the band-structure calculation and its results are given in Sec. II. The ARPES measurements and their comparison with the calculated band structure are the topics of Sec. III.

II. BAND STRUCTURE OF GeS

A. Crystal structure

GeS crystallizes in an orthorhombic structure with lattice constants $a = 4.30$ Å, $b = 3.64$ Å, and $c = 10.47$ Å. The unit cell contains four molecules with atoms in the coordinate positions

$$\pm(u, \tfrac{1}{4}, w); \pm(\tfrac{1}{2} - u, \tfrac{1}{4}, \tfrac{1}{2} + w).$$

The most recent structure determination[6] yielded the following values for u and w:

$$u(\mathrm{Ge}) = 0.127a, \quad w(\mathrm{Ge}) = 0.122c,$$

$$u(\mathrm{S}) = 0.499a, \quad w(\mathrm{S}) = -0.151c.$$

The atoms are arranged in double layers with a distorted cubic structure. The unit cell covers two adjacent double layers. Within a layer, each atom has three nearest neighbors, at nearly identical bond distances of 2.44 Å (1 neighbor) and 2.45 Å (2 neighbors), and two next-nearest neighbors at distances of 3.26 Å. Bonding between adjacent layers is provided by a sixth long bond of 3.28 Å. This leads to the layered structure of GeS perpendicular to the c axis which is reflected by the marked anisotropy of its physical properties. A coordination number of three contrasts with the sixfold coordination found in the isoelectronic lead salts. It must however be realized that a threefold coordination is also found in the homopolar analogs of GeS, As, Sb, and Bi, in compliance with Bradley and Hume-Rothery's "$8 - N$ rule" which states that an atom with valency N has $8 - N$ close neighbors. In this sense, GeS is a more typical IV-VI compound than are the better known lead salts.

The space group of GeS is the nonsymmorphic group D_{2h}^{16}. Figure 1 shows the orthohombic Brillouin zone (BZ) of GeS. We follow the notation of

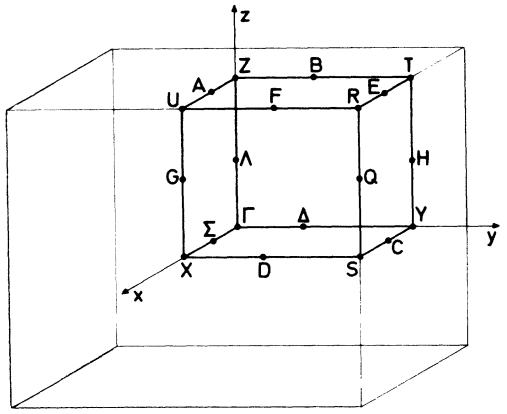

FIG. 1. Brillouin zone for a simple orthorhombic Bravais lattice, e.g., GeS.

Slater[7] in labeling the axes and symmetry points. In this convention the x, y, and z direction correspond to the c, b, and a axes, respectively.

The symmetry properties of the space group D_{2h}^{16} lead to two-dimensional irreducible representations at the corners of the irreducible $\frac{1}{8}$ of the BZ, except at Γ and U. Taking the symmetry of states under time reversal into account leads to numerous degeneracies in addition to the ordinary Kramers degeneracy as pointed out by Gashimzade.[8] A summary of the symmetry properties of the k-vector groups is set out in Table I.

It is worth noting that the edge Q of the BZ, including points R and S, is fourfold degenerate despite the low symmetry of GeS. (The space group D_{2h}^{16} only contains eight symmetry operations). The only nondegenerate symmetry points are found in the interior of the BZ, including its center Γ.

As a consequence of the rather long bond distances between adjacent double layers one might neglect the interaction between them in first order. The corresponding diperiodic space group of a separate double layer is C_{2v} and its unit cell consists of two molecules of GeS. Because C_{2v} contains less symmetry operations then D_{2h}^{16}, different irreducible representations of the latter group correspond

TABLE I. Symmetry properties of D_{2h}^{16}.

Symmetry designation	k vector	Symmetry operations of the group of k	Degeneracy by space-group symmetry alone	Actual degeneracy including time-reversal symmetry	Additional degeneracies due to time-reversal symm.
Γ	$(0,0,0)$	E, C_{2x}, C_{2y}, C_{2z}, I, IC_{2x}, IC_{2y}, IC_{2z}	1	1	...
Σ	$(P_1,0,0)$	E, C_{2x}, IC_{2y}, IC_{2z}	1	1	...
A	$(P_1,0,\frac{1}{2})$		1	2	A_1A_2, A_3A_4
C	$(P_1,\frac{1}{2},0)$		1	2	C_1C_4, C_2C_3
E	$(P_1,\frac{1}{2},\frac{1}{2})$		1	2	E_1E_3, E_2E_4
Δ	$(0,P_2,0)$	E, C_{2y}, IC_{2x}, IC_{2z}	1	1	...
B	$(0,P_2,\frac{1}{2})$		2	2	...
D	$(\frac{1}{2},P_2,0)$		2	2	...
F	$(\frac{1}{2},P_2,\frac{1}{2})$		1	2	F_1F_2, F_3F_4
Λ	$(0,0,P_3)$	E, C_{2z}, IC_{2x}, IC_{2y}	1	1	...
G	$(\frac{1}{2},0,P_3)$		1	2	G_1G_4, G_2G_3
H	$(0,\frac{1}{2},P_3)$		2	2	...
Q	$(\frac{1}{2},\frac{1}{2},P_3)$		2	4	Q_1Q_1
X	$(\frac{1}{2},0,0)$	E, C_{2x}, C_{2y}, C_{2z}, I, IC_{2x}, IC_{2y}, IC_{2z}	2	2	...
Y	$(0,\frac{1}{2},0)$		2	2	...
Z	$(0,0,\frac{1}{2})$		2	2	...
S	$(\frac{1}{2},\frac{1}{2},0)$		2	4	S_1S_2
T	$(0,\frac{1}{2},\frac{1}{2})$		2	2	...
U	$(\frac{1}{2},0,\frac{1}{2})$		1	2	U_1U_2, U_3U_4, U_5U_6, U_7U_8
R	$(\frac{1}{2},\frac{1}{2},\frac{1}{2})$		2	4	R_1R_2

TABLE II. Relationships between the irreducible representations of the three-dimensional group D_{2h}^{16} and the two-dimensional group C_{2v}.

Symmetry designation	Symmetry operations of the group of k	Irreducible representations of D_{2h}^{16} which are equivalent in C_{2v}
Γ	E, C_{2z}, IC_{2x}, IC_{2y}	$\Gamma_1=\Gamma_8$, $\Gamma_2=\Gamma_7$, $\Gamma_3=\Gamma_6$, $\Gamma_4=\Gamma_5$
Σ		$\Sigma_1=\Sigma_2$, $\Sigma_3=\Sigma_4$
A	E, IC_{2y}	...
C		$C_1C_4=C_2C_3$
E		$E_1E_3=E_2E_4$
Δ		$\Delta_1=\Delta_2$, $\Delta_3=\Delta_4$
B		...
D	E, IC_{2x}	...
F		$F_1F_2=F_3F_4$
Λ		...
G		...
H	E, C_{2z}, IC_{2x}, IC_{2y}	...
Q		...
X		...
Y		$Y_1=Y_2$
Z		...
S	E, C_{2z}, IC_{2x}, IC_{2y}	...
T		$T_1=T_2$
U		$U_1U_2=U_7U_8$, $U_3U_4=U_5U_6$
R		...

to one irreducible representation in C_{2v} in some cases. The ones that become equivalent in case of no interactions between different double layers are summarized in Table II.

B. Band-structure calculation

The band structure of GeS was calculated using the energy-independent local pseudopotential formalism and neglecting spin-orbit interaction. A detailed description of this method is given in Ref. 9. Here we only summarize the formulas that define the form factors. The pseudopotential $V(\vec{r})$ which enters the pseudo-Hamiltonian $H=-\nabla^2+V(r)$ (in a.u.) possesses the translational symmetry of the crystal lattice and can therefore be expanded into a Fourier series

$$V(\vec{r})=\sum_{\vec{G}} V(\vec{G})\exp(i\vec{G}\cdot\vec{r}), \tag{1}$$

with the summation extending over all reciprocal-lattice vectors $\vec{G}$. The Fourier transforms $V(\vec{G})$ are defined by

$$V(\vec{G})=\frac{1}{N}\sum_{j=1}^{N}\exp(-i\vec{G}\cdot\vec{u}_j)v_j(\vec{G}). \tag{2}$$

The summation extends over all N atoms in the unit cell with positions $\vec{u}_j$. The atomic form factors $v_j(\vec{G})$ are normalized to the average atom volume Ω_0/N, where Ω_0 is the volume of the unit cell. The atomic pseudopotentials were taken to be spherically symmetric and the discrete values $v_j(|\vec{G}|)$ were computed from analytic functions of the form

$$v_j(q)=v_j^0(q)(q^2+a_{j1})/a_{j1}\frac{1}{1+\exp[a_{j2}(q^2-a_{j3})]}, \tag{3}$$

for $q\geq q_{j0}$, and the power series

$$v_j(q)=\sum_{n=0}^{4} b_{jn}q^n, \quad q\leq q_{j0}. \tag{4}$$

The two functions and their derivatives were matched smoothly at q_{j0}, the cutoff wave vector. $v_j^0(q)$ is the empty core pseudopotential form factor as given in Ref. 9 (p. 55).

The pseudo-Hamiltonian was diagonalized in a basis of plane waves taking full advantage of the symmetries of the wave-vector groups. Plane waves with $|\vec{k}+\vec{G}|^2\leq E_1=70$ eV were included exactly. That corresponds to a total number of about 250 plane waves. The convergence of the energy levels was checked extending the basis set to 500 plane waves. The convergence was found to be better than 0.2 eV in a 10-eV wide band around the fundamental gap with the value chosen for E_1.

An initial set of form factors for Ge and S was obtained by fitting expressions (3) and (4) to the form factors given by Cohen and Heine.[9] Corrections had to be made, however, in the small-q regime to bring the calculation in reasonable agreement with the photoemission data and the 1.65-eV gap of GeS. The particularly large extension of the GeS unit cell in the x direction requires form factors in a q regime not normally

TABLE III. Parameters used in the EPM calculations.

	Ge	S
R_c	1.61	1.83
a_1	4.55	14.40
a_2	2.11	3.45
a_3	3.92	4.13
b_0	−0.029 17	0.000 80
b_1	0.019 23	−0.148 38
b_2	0.029 07	0.163 64
b_3	0.004 40	−0.052 57
b_4	−0.005	0.004

used. The final set of parameters used to calculate $v_j(q)$ is listed in Table III.

The band structure of GeS is plotted along the edges of the two faces of the irreducible eighth of the BZ which are normal to the basal plane $x = 0$ of the GeS unit cell. These are the directions that will be used in discussing the results of our ARPES measurements. Energies are referred to the top of the valence bands. The four valence electrons of Ge($4s^2 4p^2$) and the six valence electrons of S($3s^2 3p^4$) add up to a total of 40 valence electrons per unit cell of GeS which fill the 20 lowest nondegenerate bands in Figs. 2 and 3. The unoccupied conduction bands are separated from these by a direct gap of 1.2 eV along the Λ line.

Following an extreme linear combination of atomic orbitals (LCAO) approach that neglects s-p hybridization we can classify the valence bands according to the following scheme. The two groups of four bands each around −19 and −9 eV are the band-structure analogs of the S(3s) and the Ge(4s) levels, respectively. The remaining 12 valence bands are derived from bonding combinations of the S(3p) and Ge(4p) atomic orbitals. This classification scheme reflects reality, however, for the sulfur s bands only, which are well separated from the rest of the bands and show little dispersion. Towards higher energies, atomic orbitals hybridize considerably and the above designations are only approximations.

In agreement with the previous discussion of degeneracies along various symmetry lines (cf. Table I), we observe only ten filled (and double degenerate) bands along the lines D, C, A, G, and at the points X, Y, Z, U, and only five occupied (and fourfold degenerate) levels at point S.

A remarkable feature of the band structure may be found along lines Δ and Λ, especially for the s-derived bands: We observe pairs of bands that are nearly parallel to each other. The splitting within a pair is only 0.3 eV for the S(3s) bands and 0.9 eV for the Ge(4s) bands. One can easily

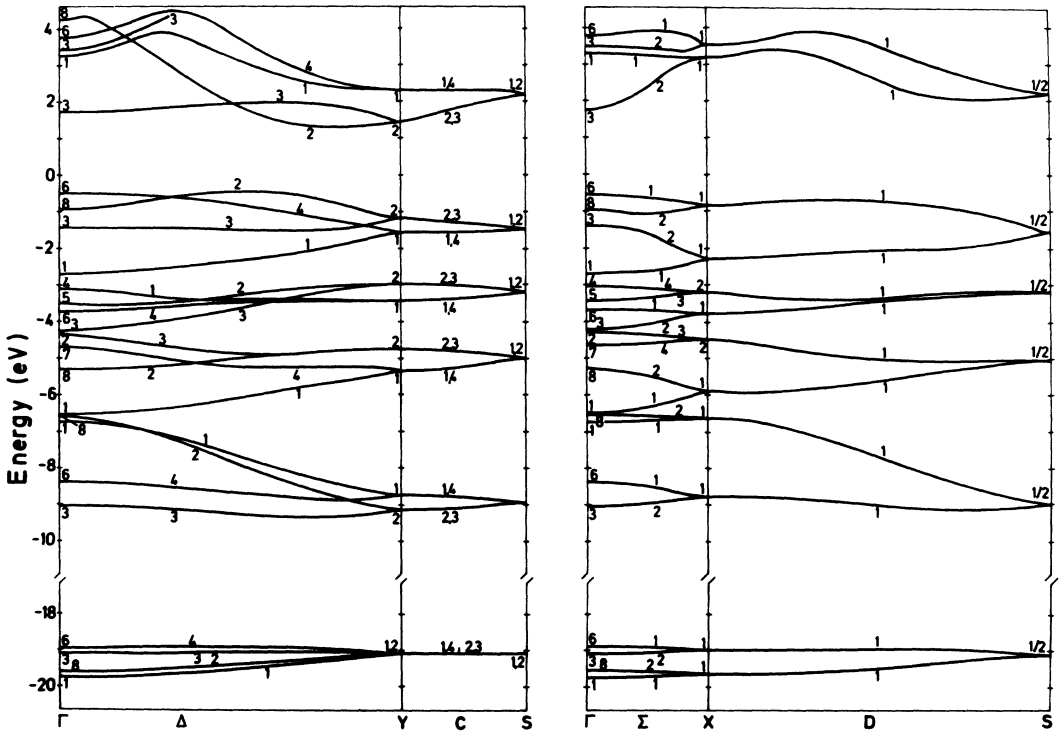

FIG. 2. Band structure of GeS calculated along symmetry lines Δ, C, Σ, D.

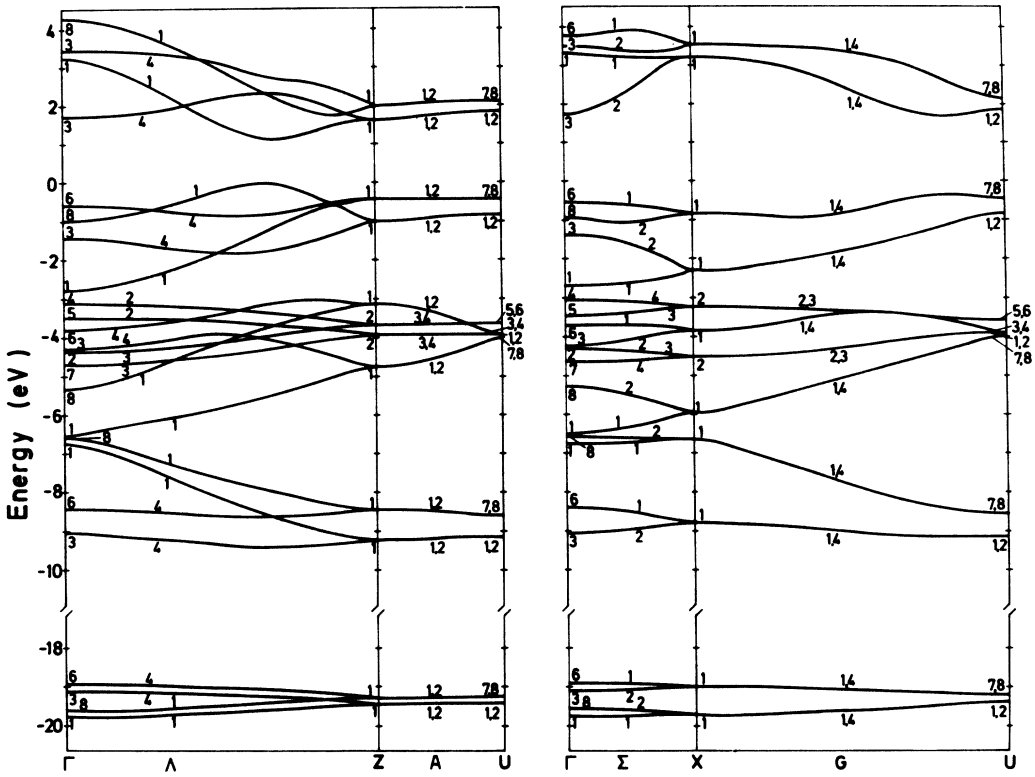

FIG. 3. Band structure of GeS calculated along symmetry lines Λ, A, Σ, G.

see that this splitting is caused by electronic interactions between the double layers of the GeS structure. If there were no interaction, all bands should be flat in the k_x direction. Consequently, the bands along D and Δ should be identical, e.g., the lowest D_1 should have the same dispersion as the "combined" Δ_1/Δ_2. The same argument applies to all higher bands along D and Δ, although it is not always trivial to find the related pairs because of numerous crossings.

These observations are consistent with the results of our group theoretical analysis (cf. Table II). If the double layers may be treated separately, the number of states is reduced by a factor of 2, and states that were different on the two layers of the three-dimensional unit cell but are equivalent in the two-dimensional representations have to merge. Δ_1 and Δ_2 as well as Δ_3 and Δ_4 are equivalent representations.

A careful inspection of lines G and Λ (Fig. 3) which should also be identical yields that a fourfold degeneracy along line A is necessary in some cases to provide flatness of all bands in the k_x direction. This is at least true for all s-derived bands, but not for those bands just below the fundamental gap. Yet the equivalence of representations U_1U_2 and U_7U_8 in C_{2v} establishes a fourfold degeneracy of all bands along A.

The—at least—double degeneracy of all bands as a consequence of the absence of electronic interactions between adjacent double layers permits a simple physical interpretation. As mentioned in Sec. II A, the unit cell of GeS covers two successive double layers, which are identical apart from a different orientation in space. That means that the two double layers should reveal the same band structure if there were no electronic interactions between them, and that explains the double degeneracy of all energy bands in that case.

By arguing the other way round we suggest that the amount of splitting is a measure of electronic interactions between different double layers.

III. PHOTOEMISSION MEASUREMENTS

A. Experimental

Experiments were performed in a commercially available angle-resolving photoelectron spectrometer in which the electron energy analyzer can be rotated about the sample. An independent rotation of the sample around two mutually perpendicular axes gives an almost complete freedom in the choice of directions for the electrons to be analyzed and the exciting photon beam relative to

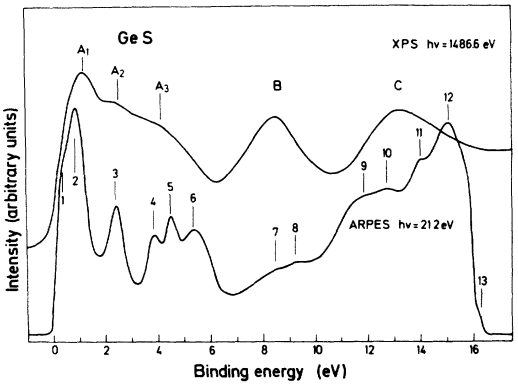

FIG. 4. x-ray ($h\nu = 1486.6$ eV) induced and angular-resolved uv ($h\nu = 21.2$ eV, $\theta_e = 0°$, $\theta_\omega = -45°$) induced photoemission spectra of GeS.

the surface normal of the sample. The only restriction is a coplanar arrangement of photon beam and the electron acceptance direction. That limits the angle between these two to a range from ~15° to ~215°. A system to observe low-energy electron diffraction (LEED) is incorporated in the same ultrahigh-vacuum envelope.

Single crystals of GeS, grown by vacuum sublimation[10] were cleaved along the basal planes *in vacuo* ($p = 2\times10^{-10}$ Torr) to yield surfaces of mirror finish. *In situ* analysis of the freshly cleaved surfaces by LEED insured a surface periodicity in agreement with the two-dimensional projection of the bulk unit cell and allowed a proper selection of the azimuthal angle for the subsequent photoemission measurements. Measurements were limited to surfaces with the sharpest possible diffraction patterns which guaranteed a coherence area of the surface periodicity that is necessary for the conservation of parallel momentum in the hot electron transmission through the topmost layers of the crystal.

ARPES measurements were performed at an angular resolution of 3° (opening angle of electron analyzer acceptance cone) and an energy resolution of 0.2 eV. A differentially pumped He-discharge lamp delivered photons of energy $h\nu = 21.22$ eV (He I resonance).

B. Results

In this section we present our measurements and discuss them on a level that makes optimal use of the symmetry properties of the crystal and the basic assumptions of the conservation of $\vec{k}_\parallel$. A detailed comparison with the band-structure calculation presented above will be given in Sec. III D.

Polar angles will be referred to as θ_e and θ_w for the electron and light direction, respectively. They are measured relative to the surface normal of the sample. The reproducibility of these angles is ±0.5° and their absolute accuracy is estimated to be ±1.5°. The same holds for the azimuthal angle which is kept constant for one series of measurements.

Figure 4 shows a total photoelectron spectrum at $\theta_e = 0°$ and $\theta_w = 45°$. Binding energies are measured relative to the intersection of the line of steepest descent of the leading edge with the base line. We will refer to this point in a loose manner as the top of the valence band. The total width of the spectrum is 16.0 eV and the photoelectric threshold is therefore 5.2 eV. Also shown in Fig. 4 is an angle integrated spectrum taken from Ref. 5. It was measured with $h\nu = 1486.6$ eV (monochromatized Al $K\alpha$). The increase in fine structure in going from this spectrum to the angularly resolved case is apparent.

Using the x-ray-induced spectrum (XPS) which gives a fair replica of the density of occupied states we shall organize the multitude of peaks in the ARPES into three groups: The first group of six peaks extending from 0- to 6-eV binding energy falls under the peak of high density labeled *A* in Fig. 4. These peaks represent electrons in bands which are derived from bonding combinations of predominantly Ge($4p$) and S($3p$) electrons. We shall therefore refer to these bands as p bands. Peak *B* in the XPS spectrum covers peaks 7 and 8 in the ARPES spectrum and peak *C* covers those labeled 9–12. A kink at 14.8 eV marks the high-energy cutoff of the ARPES spectrum and the shoulder 13 arises from electrons photoemitted from the analyzer slits through stray light reflected off the sample. Because of the low intensity of the Ge($4s$) peaks and the ambiguity in identifying the S($3s$) peaks we shall limit our following discussion to the first 7-eV binding energy which cover the p bands only.

Angular-resolved spectra were taken for $\vec{k}_\parallel$ along the two principal crystal axes a and b with the photon direction fixed at angles of $\theta_w = -45°$ ($\vec{k}_\parallel$ parallel a) and $\theta_w = -55°$ ($\vec{k}_\parallel$ parallel b), respectively. The electron polar angle was varied between $\theta_e = \theta_w + 15°$ and $\theta_e = -\theta_w - 5°$ in steps of 2.5° along the b direction, and in steps of 2.0° along the a direction. Measurements beyond the upper limit were hampered by light that was specularly reflected from the sample into the analyzer. The lower limit in θ_e was set by the physical interference between the rotating analyzer and the fixed lamp.

A number of representative spectra for the two symmetry directions are shown in Figs. 5 and 6. The potential wealth of information contained in

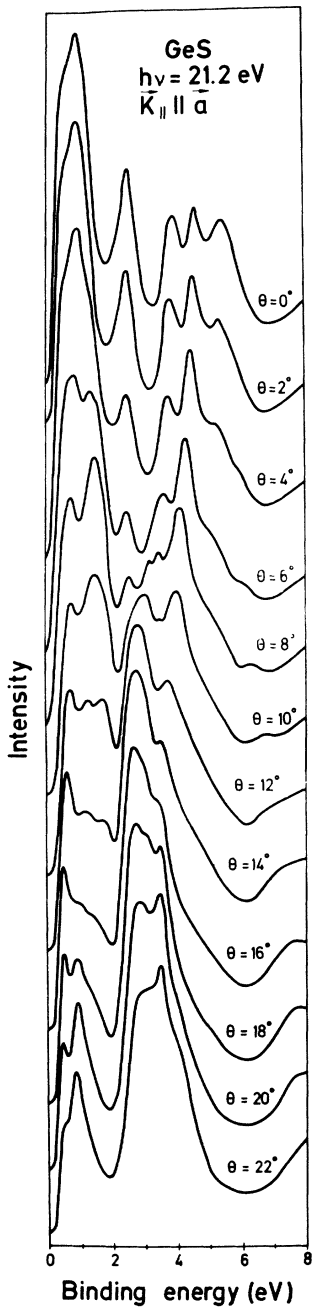

FIG. 5. Angular-resolved uv photoemission spectra for $\vec{k}_{\parallel}$ along a ($\theta_w = -45°$).

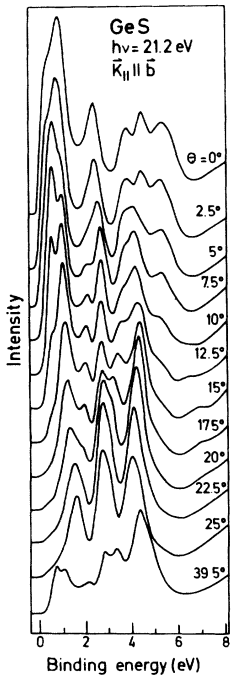

FIG. 6. Angular-resolved uv photoemission spectra for $\vec{k}_{\parallel}$ along b ($\theta_w = -55°$).

these spectra is apparent from the multitude of sharp features and their dramatic change in position and intensity within an angular range of only about 20°. The most striking difference of these spectra as compared with angle-integrated spectra lies in the fact that almost all structure appears in the form of symmetrical Gaussian-like peaks instead of continuous if structured distributions. The few complicated structures can readily be decomposed into individual peaks also. The width of the peaks varies between a maximum of about 1 eV full width at half maximum (FWHM) to values as small as 0.3 eV FWHM. In this respect the spectra resemble those taken from gases in which discrete molecular orbitals are ionized. This observation lends substantial support to the interpretation of ARPES spectra in terms of direct transitions between one-electron band states at relatively (relative to the band dispersion) well-defined points in reciprocal space.

In Figs. 7 and 8 the measured peak positions are plotted versus the projection $\vec{k}_{\parallel}$ of their momentum $\vec{k}$ onto the basal plane of crystal. $\vec{k}_{\parallel}$ was calculated from the kinetic energy E_k of the electrons under a given peak, according to

$$|\vec{k}_{\parallel}| = (2E_k)^{1/2} \sin\theta_e . \tag{5}$$

The origin of points in the so constructed E-vs-

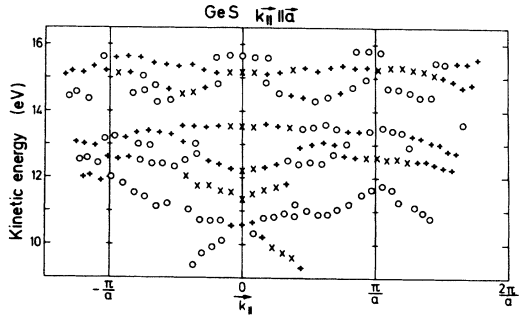

FIG. 7. Peak positions vs electron-momentum component $\vec{k}_{\parallel}$. The direction of $\vec{k}_{\parallel}$ is chosen along a.

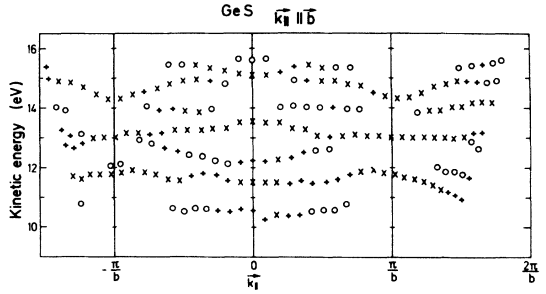

FIG. 8. Peak positions vs electron-momentum component $\vec{k}_{\parallel}$. The direction of $\vec{k}_{\parallel}$ is choosen along b.

$\vec{k}_{\parallel}$ plots is schematically indicated by symbols. Slanted crosses are taken for data points derived from well-defined peaks. Crosses stand for peaks deconvoluted from composite structures and open circles represent shoulders. The accuracy of energies decreases accordingly from typically ±0.05 eV for peaks to about ±0.2 eV for the position of weak shoulders. The uncertainties in θ_e and E_k contribute to the error in $\vec{k}_{\parallel}$, according to Eq. (5). The dominant factor, however, is the uncertainty of θ_e of ±1.5% which leads to an error in $\vec{k}_{\parallel}$ of 0.03 a.u. at $\theta_e = 0°$. That corresponds to 3% of the dimension of the BZ along a and 4% of the dimension along b, respectively.

C. Symmetry properties of the measured energy versus momentum curves

Before we attempt a detailed comparison of the measured energy-versus-momentum curves with our band-structure calculation it is useful to consider two symmetry properties of the energy-momentum curves. The BZ of GeS has three mirror planes through the center and perpendicular to the three principal axes. This mirror symmetry corresponds to a degeneracy of bands for positive and negative $\vec{k}_{\parallel}$ measured along any of these axes. In Fig. 9 we have overlayed peak positions measured for positive and negative directions of $\vec{k}_{\parallel}$ along a and b. For the b direction the two sets of data are seen to coincide almost perfectly. The deviations are smaller than 0.1-eV energy everywhere except for three points around $|\vec{k}_{\parallel}| = 0.58$ a.u. which deviate by 0.3 eV from the main line. These points are taken from the deconvolution of a composite peak and therefore fall within the error limits quoted above. We take the success of this first symmetry test as proof that residual magnetic or electrical fields in the region between sample and analyzer are small enough not to affect our spectra in a noticeable manner.

The situation for $\vec{k}_{\parallel}$ along a is basically similar to that along b. The energy-momentum curves are however more complicated for $|\vec{k}_{\parallel}| \gtrsim 0.15$ a.u. and it is therefore not always possible to find unambiguous connections between points in the form of continuous bands. This is as we shall see due to a more complicated band structure along a which leads to more overlapping peaks in the original spectra and therefore to more ambiguities in the data reduction procedure.

The second symmetry requirement relates to the reducibility of the band structure. States which differ in crystal momentum by reciprocal-lattice vectors are degenerate in energy. In our particular case, this requires that bands ought to be symmetrical around the zone boundaries $Y-S$ and $Z-U$ which are indicated by vertical lines in Fig. 9. Referring to this figure we find that this mirror symmetry holds in general for $\vec{k}_{\parallel}$ along b. Deviations occur mainly further away from the zone boundary. Most striking is a string of points which appears to connect the two lowest bands when folded back into the central BZ. A similar cross connection is found between the two top bands along a. For the remainder of the bands along a the symmetry seems to hold quite well within the qualifications made earlier for this direction.

These new bands may be explained by considering the perpendicular wavevector component $k_{\perp}$ of the states involved in the electronic transition. The periodicity of the cyrstal surface relates the parallel component $\vec{k}_{\parallel}$ of the outgoing plane wave directly to the corresponding component $\vec{k}_{0\parallel}$ of the final state ψ_f inside the crystal.

A proper framework for the determination of $k_{\perp}$ is set by the theory of low-energy electron diffraction (LEED)[11] if we follow the idea of Feibelman and Eastman[12] who treat the final state in photoemission as the time-reversed initial state in a LEED experiment.

Let us consider the special case of an orthorhombic lattice without any reconstruction of the

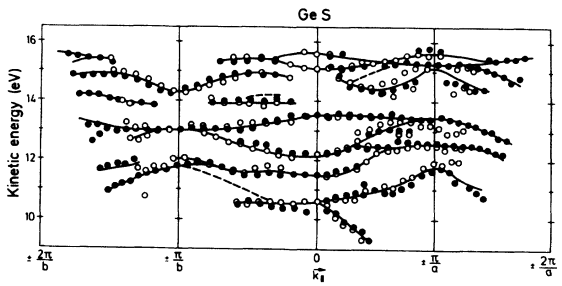

FIG. 9. Comparison of peak positions for positive (full circles) and negative (open circles) $\vec{k}_{\parallel}$. Experimental points are connected to give energy vs momentum curves that satisfy basic symmetry requirements (for details see text).

surface, a situation most likely true for GeS as indicated by the observed rectangular LEED pattern. Solving the initial state LEED problem will then reduce to two steps: (i) solution of the Schrödinger equation for states with energy $E_f = E_i + h\nu$ and parallel wave-vector component $\vec{k}_{0\parallel}$; (ii) matching of the eigenfunctions thus obtained to the amplitude a_g of an incoming plane wave $a_g \exp(i\vec{p}_g \cdot \vec{r})$,

$$\vec{p}_g = (\vec{k}_{0\parallel} + \vec{g}, (2E - |\vec{k}_{0\parallel} + \vec{g}|^2)^{1/2})$$

at the surface ($x = 0$). Here $\vec{k}_{0\parallel}$ is the parallel momentum component of $\vec{p}_g$, reduced to lie in the first two-dimensional BZ, and $\vec{g}$ is any two-dimensional reciprocal-lattice vector, and a_g the amplitude of the plane wave just inside the surface barrier.

The Hamilton operator of the excited electron in the crystal is expressed in terms of plane waves running in opposite directions towards the surface which have momenta

$$\vec{K}_g^{\pm} = ((\vec{k}_{0\parallel} + \vec{g}), \pm(2E_f - |\vec{k}_{0\parallel} + \vec{g}|^2)^{1/2})$$

and amplitudes $b_g^{\pm}$. Imposing a Bloch wave condition on these amplitudes in the direction perpendicular to the surface

$$b_g^{\pm}(x + c) = b_g^{\pm}(x) \exp(i k_\perp c)$$

diagonalizes the Hamiltonian to give a set of eigenvalues $k_\perp$ and corresponding eigenvectors $b_{gk_\perp}^{\pm}$. This procedure is, of course, equivalent to solving the band-structure problem which solves for E at a given $\vec{k}$ whereas we solve for $k_\perp$ at a given $\vec{k}_{0\parallel}$ and E.

The matching procedure requires that the amplitudes $b_{gk_\perp}^{+}(x = 0)$ add to give the correct incident wave at the surface

$$a_g = \sum_{k_\perp} A(k_\perp) b_{gk}^{+}(x = 0).$$

The interpretation of this equation in terms of the photoemission process requires that final states ψ_f of the optical excitation are given by

$$\psi_f = \sum_{k_\perp} A(k_\perp) \sum_g b_{gk_\perp}^{+}(x = 0) \exp(i \vec{K}_g^{+} \cdot \vec{r})$$

This has the following consequences for the interpretation of our spectra:

(i) For a given observed beam of electrons with energy E and $\vec{k}_{\parallel} = \vec{k}_{0\parallel}$ there will be a number of possible $k_\perp$ at which the optical transitions take place that contribute to the intensity of this beam.

(ii) The same set of $k_\perp$ values contributes to all beams differing in $\vec{k}_{\parallel}$ by two-dimensional reciprocal-lattice vectors.

(iii) The amplitude with which a transition $\psi_i \rightarrow \psi_f(\vec{k}_{0\parallel}, k_\perp)$ will contribute to beams of different $\vec{g}$ is determined by the product $A(k_\perp) b_{gk_\perp}^{+}(x = 0)$. It is therefore possible that the beam at $\vec{k}_{\parallel}$ couples predominantly to one $k_\perp$ and the beam at $\vec{k}_{\parallel} + \vec{g}$ couples to a different $k_\perp$. This would therefore explain the new bands observed in the second zone along a and b.

The possible eigenvalues $k_\perp$ will in general be complex due to the finite lifetime of the hot electron. As pointed out by Feibelman and Eastman this leads to a range of optical transitions around $\mathrm{Re}k_\perp$ with a width given by $\mathrm{Im}k_\perp$ for any given value of $\vec{k}_{\parallel}$. An order of magnitude estimate of $\mathrm{Im}k_\perp$ is obtained from the observed mean free paths in photoemission which do not differ too much from material to material. For 12-eV electrons this mean free path is about 10 Å according to the compilation of Lindau and Spicer.[13] This corresponds to a value of $\mathrm{Im}k_\perp \approx 0.2$ Å^{-1} or about $\frac{1}{3}$ of the irreducible half of the BZ of GeS in the direction perpendicular to the layers. An ARPES spectrum corresponds approximately to the energy dispersion ΔE of the *initial state* over the range of $\mathrm{Im}k_\perp$.

Let us consider as an example the three peaks observed along b for $\vec{k}_{\parallel}$ corresponding to the edge of the BZ. The initial states contributing to these peaks are the fourfold-degenerate points S and states along the line $S - Y$. The measured width of the peaks in 0.6 ±0.1 eV (FWHM) compared to a total dispersion of 0.4–0.6 eV along $S - Y$, which is slightly less than expected but still satisfactory considering the crudeness of our estimate.

D. Comparison of experimental E-vs-$\vec{k}_{\parallel}$ curves with the band-structure calculation

In Fig. 10 we compare our experimental results with the band-structure calculation for GeS. The points of Fig. 9 have been connected by continuous lines to yield experimental E-vs-$\vec{k}_{\parallel}$ curves. The experimental bands are set next to their theoretical counterparts along Γ-Δ-Y and Γ-Λ-Z, respectively. The selection of these lines rather than the corresponding lines X-D-S and X-G-U on the face of the BZ for the comparison is based on the one-dimensional density of states along $k_\perp$. Referring back to Figs. 2 and 3 one finds that each state along X-D-S and X-G-U splits into two approximately symmetrical bands along $k_\perp$. They reach their maximum separation with zero gradient at $k_\perp = 0$ along the lines Γ-Δ-Y and Γ-Λ-Z.

The one-dimensional density of states associated with these bands has characteristic singularities at the endpoints and a region of low density in the middle. These sharp maxima ($\Delta E \approx 0.1$ eV) in the density of states are most likely to be picked up under the conditions explained in Sec. III C. Their

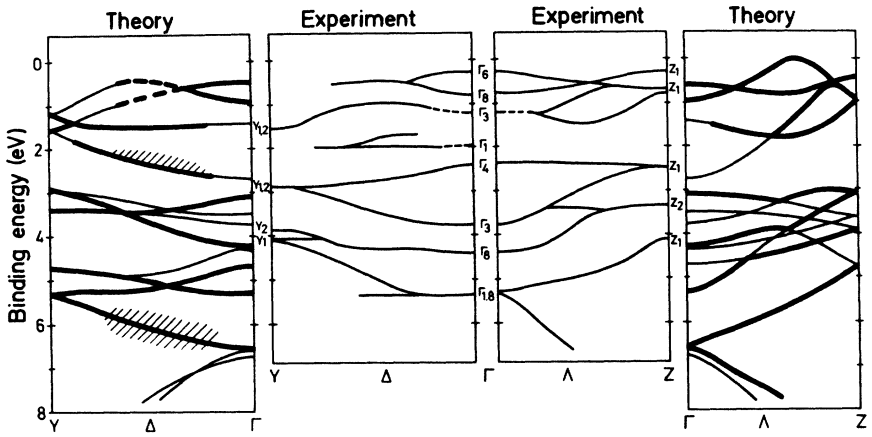

FIG. 10. Comparison of experimental and calculated band structure of GeS. Those portions of the calculated bands which correspond to the measured E-vs-$\vec{k}_{\parallel}$ curves are marked by bold lines. Hatched regions indicate cases in which we suggest that transitions at $k_{\perp} \neq 0$ are the origin of the peaks.

energies are practically identical with the positions of the calculated bands shown in Fig. 10.

In this figure, those portions of the calculated bands which correspond to the measured E-vs-$\vec{k}_{\parallel}$ curves are marked by bold lines. Hatched regions indicate cases in which we suggest that transitions at $k_{\perp} \neq 0$ are the origin of the observed peaks. These identifications are based on four criteria:

(i) The p bands of GeS are divided into three groups of bands. The bands of each group are connected to one of the three symmetry points (S points) at 1.50, 3.20, and 5.00 eV below the top of the valence bands. Along the b direction these groups do not overlap and we can deal with them separately. In the a direction this holds only for the top group and the two lower groups together.

(ii) We assume that the level ordering of the calculation is correct at least to within the experimental resolution of about ±0.2 eV. This is supported by the great stability of the level ordering under variations of the pseudopotential.

(iii) The assignment of E-vs-$\vec{k}_{\parallel}$ curves has to be consistent with the continuity of these bands across Γ, the center of the BZ. This puts additional constraints on possible alternatives and helps in the assignments.

(iv) The shape of the bands, their position relative to each other, and points of degeneracy have to agree in theory and experiment.

We feel that the assignments made on the basis of these criteria describe the experimental data in terms of the band structure quite well. This is especially true for the top group of bands and the lowest two or three bands where an almost one-to-one correspondence is observed. We have already commented on the cross connection between the two lowest bands along b which cannot be explained on the basis of the one-dimensionsl density of states alone. The identification of bands Δ_4 and Δ_3 around 3-eV binding energy is not to be taken literally in view of the complexity of the bandstructure as well as the measurements in this region.

The assignments of symmetry points based on the outlined procedure are indicated in Fig. 10 and their energies are compared with the calculated energies in Table IV. Also listed in Table IV are the energies of the S points. The experimental values are taken from the peak positions A_1, A_2, A_3, B, and C in the XPS spectrum as

TABLE IV. Measured and calculated binding energies (eV) relative to the top of the valence band of identified symmetry points.

Symmetry point	E_B (Calc.)	E_B (ARPES)	E_B (XPS)
Γ_6	0.50	0.30	
Γ_8	0.90	0.90	
Γ_3	1.40	(1.10)	
Γ_1	2.70	(1.90)	
Γ_4	3.05	2.35	
Γ_3	4.25	3.70	
Γ_8	5.30	4.40	
Γ_1/Γ_8	6.50	5.40	
Z_1	0.45	0.45	
Z_1	1.00	0.90	
Z_1	3.10	2.55	
Z_2	3.90	3.30	
Z_1	4.75	4.05	
Y_2	1.20	1.55	
Y_1	1.60		
Y_2	2.95	2.90	
Y_1	3.40		
Y_2	4.75	3.85	
Y_1	5.35	4.15	
S_1S_2	1.50		1.2
S_1S_2	3.20		2.4
S_1S_2	5.00		4.2
S_1S_2	8.95		8.5
S_1S_2	19.10		13.1

labeled in Fig. 4. States around S are bound to contribute substantially to the density of states because of their high degeneracy, the small energy dispersion of bands around S, and because of their position at a corner of the BZ with its high associated volume. States at S are therefore expected to show up dominantly in the XPS spectrum.

The deviations between theoretical and experimental energies increase from less than 0.2 eV near the top to about 1.0 eV at the bottom of the p bands and to even 6 eV for the S(3s) derived bands. We attribute this discrepancy to the local pseudopotential used in our calculations. It could be fixed by using an effective electron mass slightly bigger than 1.

The gap between low-energy ARPES and high-energy XPS is bridged by the close agreement of the first three $S_{1,2}$ binding energies as derived from peaks A_1, A_2, and A_3 in XPS on one side and the energies of the corresponding Y_1, Y_2 doublet from the ARPES data, on the other hand. This is, of course, expected on the basis of the band-structure calculation.

ACKNOWLEDGMENTS

It is a pleasure to thank D. Schiferl, M. Cardona, A. Frey, and S. Rabii for must useful discussions. We thank W. Stetter and E. Schönherr for growing the single crystals of GeS.

[1]E. O. Kane, Phys. Rev. Lett. 12, 97 (1964).
[2]See e.g., N. V. Smith, M. M. Traum, and F. J. Di Salvo, Solid State Commun. 15, 211 (1974); P. K. Larsen, G. Margaritondo, J. E. Rowe, M. Schlüter, and N. V. Smith, Phys. Lett. A 58, 423 (1976).
[3]See, e.g., N. V. Smith and M. M. Traum, Phys. Rev. Lett. 31, 1247 (1973).
[4]J. D. Wiley, A. Breitschwerdt, and E. Schönherr, Solid State Commun. 17, 355 (1975).
[5]P. C. Kemeny, J. Azoulay, M. Cardona, and L. Ley Nuovo Cimento (to be published).
[6]G. Bissert and K. F. Hesse (private communication).
[7]J. C. Slater, *Symmetry and Energy Bands in Crystals* (McGraw-Hill, New York, 1965).
[8]F. M. Gashimzade, Fiz. Tverd. Tela 2, 2070 (1960) [Sov. Phys.-Solid State 2, 1856 (1961)].
[9]M. L. Cohen and V. Heine, *Solid State Physics V*, edited by H. Ehrenreich, F. Seitz, and D. Turnbull (Academic, New York, 1970).
[10]E. Schönherr and W. Stetter, J. Cryst. Growth 30 (1975).
[11]J. B. Pendry, *Low-Energy Electron Diffraction* (Academic, London, 1974).
[12]P. J. Feibelman and D. E. Eastman, Phys. Rev. B 10, 4932 (1974).
[13]I. Lindau and W. E. Spicer, J. Electron. Spectrosc. Relat. Phenom. 3, 409 (1974).